Mechanochemical rules for membrane-reshaping composite filaments

Billie Meadowcroft,[1,2,3] Ivan Palaia,[1] Anna-Katharina Pfitzner,[4]
Aurélien Roux,[4,5] Buzz Baum,[6] and Anđela Šarić[1,2,3]

[1] *Institute of Science and Technology Austria, 3400 Klosterneuburg, Austria*
[2] *Department of Physics and Astronomy, Institute for the Physics of Living Systems, University College London, London WC1E 6BT, United Kingdom*
[3] *MRC Laboratory for Molecular Cell Biology, University College London, London WC1E 6BT, United Kingdom*
[4] *Biochemistry Department, University of Geneva, CH-1211 Geneva, Switzerland*
[5] *Swiss National Centre for Competence in Research Programme Chemical Biology, CH-1211 Geneva, Switzerland*
[6] *MRC-Laboratory of Molecular Biology, University of Cambridge, Cambridge CB2 1TN, United Kingdom*

(Dated: May 5, 2022)

Sequentially assembling and disassembling protein filaments of increasing curvature has been recently proposed as an operating mechanism for the ESCRT system, a prominent machinery that deforms and cuts cell membranes. We develop a kinetic model that couples filament–membrane adhesion, filament mechanics and membrane mechanics, to explain the role of staged filament assembly/disassembly and identify the physical conditions needed for it to occur. We show that sequential assembly lowers large energy barriers for membrane deformation, providing a robust method for cell reshaping.

Nanoscale filaments that can apply forces to reshape cell membranes are key for traffic, motility and healing. Recently, a family of membrane-reshaping proteins, ESCRT-III, has come into the spotlight. These proteins primarily remodel the membrane to form negatively curved surfaces [1, 2] and are involved in a range of processes, including membrane budding and cell division [3, 4]. ESCRT-III proteins form composite polymers, bound to the membrane, that dynamically exchange different subunits with the surrounding cytoplasm. The dissociation of the polymerised subunits is catalysed by ATPase Vps4, actively providing energy, while new subunits are continuously recruited from the cytoplasm and polymerise on the membrane, replacing the dissociated ones. It is believed that this mechanism gradually modifies the composition of the filament and therefore its geometry and mechanical properties, driving membrane remodelling [5–8]. This hypothesis has gained more traction from a recent set of experiments showing that ESCRT-III filaments that polymerise into membrane-bound spiral filaments, driven by Vps4 and ATP, undergo continuous and spontaneous sequential exchange of five different subunits to deform and cut the membrane [9]. An exciting interpretation is that a membrane-bound filament may shift from a preferred shape that is curved but flat, to a highly-curved three-dimensional helix via the exchange of its composite subunits, thereby causing membrane indentation [8, 10].

An obvious outstanding question is: which physicochemical properties enable different subunits to assemble and disassemble in a staged-like manner, completely *in situ*? ESCRT-III polymers have been observed to form many different shapes and to have different membrane binding interfaces [11–15]. Therefore, the different ESCRT-III subunits likely have different intrinsic curvatures, adhesion energies, binding angles to the membrane, and possibly different rigidities. Hence, an attractive hypothesis is that the timing of the assembly-disassembly of the subunits is governed by the mechanical and chemical differences between them.

Here we investigate this mechanochemical hypothesis by developing a kinetic model that can capture recruitment and spontaneous unbinding of monomers of different properties. We assume spiral- or helix-shaped filaments, as observed in experiments [9], and investigate the effect that binding energy, filament mechanical and geometrical properties, and the consumed ATP energy have on filament assembly and membrane deformation. We find design rules for staged assembly and disassembly of composite filaments that drives membrane remodelling. The process involves subunits of increasing adhesion energies, which self-assemble into helical filaments of increasing curvatures and helical pitches, however, for the process to occur reliably, their curvatures and pitches cannot be too dissimilar. We find that sequential binding and unbinding of progressively more curved filaments lowers the energy barrier for the attachment of the final, highly, curved filament. Such a process in turn produces the maximum membrane indentation depth, suggesting that this strategy might be optimal for creating dramatic membrane curvature change, like those needed for formation of tight membrane necks from flat membranes.

Model. Although ESCRT-III filaments can have as many as 11 different subunits, as is the case for animal cells [4], as a proof of principle, here we used only three types of subunits ($i = 0$, 1 or 2), Fig. 1a. We developed a lattice model where three types of monomers can bind to and unbind from the membrane and each other, forming a membrane-bound heterogeneous filament. A filament lattice site can host one monomer of each type, such that different monomer types can effectively bind side-by-side on a lattice site (Fig. 1b). Each monomer type is associated with an energy of adhesion to the membrane $-E_i^{\mathrm{adh}}$, as well as a preferred curvature c_i and a preferred pitch p_i (Fig. 1a). These are the curvatures and pitches assumed by pure membrane-bound filaments made of a

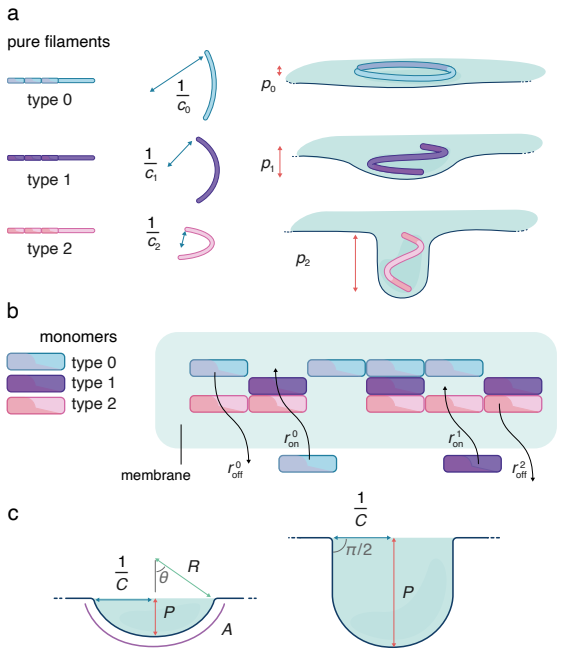

FIG. 1. **Model set up.** (a) Pure filaments made up of type-i monomers have in-plane curvature c_i and are associated with an effective pitch, p_i, causing the preferred membrane deformation depth p_i. (b) A depiction of 6 lattice sites (horizontally oriented), with the three types of monomers binding and unbinding. The unbinding rates r_{off} incorporate cost of membrane-monomer binding, filament bending, and membrane bending. (c) The overall shape of the membrane for heterogeneous filaments is determined by the composition of the filament at a given time, which gives an average pitch P and an average radius $1/C$. For a shallow pitch and large radius the geometry is that of a spherical cap, while with increasing pitch or decreased radius a tube with a spherical cap end forms.

single kind of monomer. A heterogeneous filament is associated with a non-zero filament bending energy, which results from monomers of different preferred curvatures binding to the same site or to neighbouring sites, causing frustration. For simplicity, we assume equal rigidities κ for the three monomer types. The filament curvature C is calculated as an average of the preferred curvatures c of its constituting monomers, and the pitch P as an average of the monomer preferred pitches p. Curvature and pitch define the helicoidal geometry of the filament. Fig. 1a shows the case in which the pure filament of type 0 is a completely flat spiral ($p_0 = 0$) of a curvature c_0 , whereas filaments of types 1 and 2 are helices with gradually larger pitches and curvatures ($0 < p_1 < p_2$ and $c_0 < c_1 < c_2$). We assume that the membrane adapts to the filament geometry, forming either a spherical cap or, for tight long helices, a closed tube. This is determined by the average filament curvature C and pitch P, that we use to approximate, respectively, the radius and the depth of the indentation and calculate the energy due to membrane bending (Fig. 1c).

To investigate the dynamics of the system, we introduce effective equilibrium kinetics through Monte Carlo simulations. Monomers bind or unbind according to rates r_{on} and r_{off} (Fig. 1b), which are controlled by the local filament energy, and can be enhanced through the external energy input. We focus on a situation where monomer concentrations in the cytoplasm are constant, so that binding rates are constant. The probability of a given unbinding event (i.e. involving a given site and subunit) depends exponentially, through standard statistical mechanics, on the energy change associated with it. This energy difference has three contributions, as mentioned above: monomer-membrane adhesion energy, filament bending energy, and membrane bending energy. Namely, unbinding is always penalised by adhesion, but can be favoured by filament bending if it relaxes filament frustration and by membrane bending if it reduces membrane indentation.

The length scale for our system is set by the reported curvature of Snf7 [11], an ESCRT-III subunit found in yeast that polymerizes into spirals of a radius of $\sim 30\,\text{nm}$ and represents our monomer 0. Membrane rigidity, set to $20\,k_{\text{B}}T$ [16], provides the energy scale. Monomer rigidity is compared with indirect experimental estimates of ESCRT persistence lengths [12, 17]. The remaining monomer curvatures, pitches and binding energies are parameters that we vary, within a range of physiologically plausible values. A detailed model explanation is provided in the SI.

Minimal design rules. Recent experiment [9] followed the composition of yeast ESCRT-III filaments in time, through fluorescence measurements *in vitro*, and found a series of ordered monomer peaks (Fig. 2e). Such measurements demonstrated sequential assembly-disassembly behaviour of the subunits, with the unbinding occurring in the same order as the binding, suggesting that subunits gradually replace each other as the dominant component of the filament on the membrane. Our first task is to find the conditions that can enable subunits to bind and unbind sequentially, transforming the membrane from a flat to highly curved geometry.

Within our kinetic model, we run Monte Carlo simulations exploring a range of values for the binding energies, curvatures and pitches of the 3 monomer types. We quantify how much of each monomer type is present on average in the filament as a function of time, similar to the experimental fluorescence curves.

As shown in Fig. 2b, we find that sequential monomer binding emerges only when monomers are assigned different pitches, irrespective of their curvatures and binding energies; flat monomer 0 binds before low-pitch monomer 1, which binds before high-pitch monomer 2. Helix-shaped filaments need to be bound at the end of the process to indent the membrane. However, at time 0, the membrane is flat, so that binding of high-pitch subunits is penalised. In this sense, the initial state of the membrane creates a time asymmetry and dictates the ordering of binding. The reaction progresses until the membrane

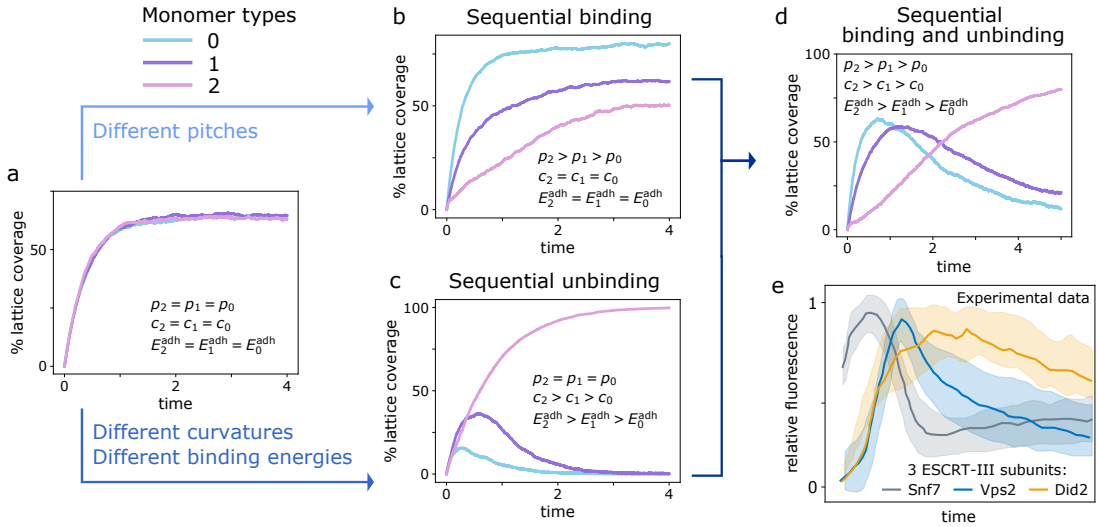

FIG. 2. **Minimal rules.** The effect of the choice of the pitches, curvatures and binding energies for the 3 types of monomers on the filament composition (% lattice coverage). When monomers are all equal (a) the filament stabilises as a composite mixture of the 3 monomers in equal parts. When the monomer types have differences in pitch (b), the binding of high-pitch subunits is delayed. Differences in curvature and adhesion energy together (c) result in the unbinding of weak-binding monomers, due to bending frustration. (d) Differences in pitch, curvature and adhesion energy are all three needed to achieve sequential assembly and disassembly. Choice of parameters: equal pitches (a and c), $p_0 = p_1 = p_2 = 0\,\mathrm{nm}$; otherwise (b and d), $p_0 = 0\,\mathrm{nm}$, $p_1 = 30\,\mathrm{nm}$, $p_2 = 45\,\mathrm{nm}$. Equal curvatures (a and b), $c_0 = c_1 = c_2 = (15\,\mathrm{nm})^{-1}$ and $E_0^{\mathrm{adh}} = E_1^{\mathrm{adh}} = E_2^{\mathrm{adh}} = 6.5\,k_{\mathrm{B}}T$; otherwise (c and d), $c_0 = (30\,\mathrm{nm})^{-1}$, $c_1/c_0 = 2.5$, $c_2/c_0 = 8$, and $E_0^{\mathrm{adh}} = 6.5\,k_{\mathrm{B}}T$, $E_1^{\mathrm{adh}}/E_0^{\mathrm{adh}} = 3$, $E_2^{\mathrm{adh}}/E_0^{\mathrm{adh}} = 12$. Time is in units of 10^3 simulation steps. (e) Experimental data showing sequential binding and unbinding of three subunits adapted from [9].

deformation energy is balanced out by monomer adhesion energy. In summary, for the sequential binding to occur in the order $0 \to 1 \to 2$, $p_2 > p_1 > p_0$ must be satisfied.

As for the sequential unbinding, we find that this is a consequence of monomer frustration within a filament. If the preferred shape of a particular monomer is very different from the local average filament shape, the monomer pays a substantial cost in elastic energy and will likely unbind. For this effect to cause asymmetric unbinding of the subunits, one monomer type must be favoured: this is the case if the monomers also have different binding energies, as shown in Fig. 2c. The monomer type with highest adhesion energy ends up dominating and eventually forcing the other two off the membrane. Conversely, the first monomer to unbind must have the smallest adhesion energy and a curvature most different from the monomer type last to be bound, so that it is forced off the membrane first. Hence, for unbinding to occur in the order $0 \to 1 \to 2$, $c_2 > c_1 > c_0$ and $E_2^{\mathrm{adh}} > E_1^{\mathrm{adh}} > E_0^{\mathrm{adh}}$ must be satisfied. The sequential disassembly fails if the subunits' curvatures are too dissimilar, in which case prohibitive filament frustration causes monomers to unbind as soon as they bind. Taken together the minimal design rules that are required to obtain sequential subunit exchange are the following: increasing pitch, increasing adhesion energy and increasing curvature (see Fig. 2d). Failure in satisfying any of these three criteria hinders sequentiality in binding or unbinding with the robustness of this behaviour further quantified in Fig. S2.

Role of sequential binding/unbinding. To explain why the sequential assembly/disassembly is needed, we now analyse different possible pathways to the final membrane-wrapped tight helix configuration. Using the parameters that result in sequential assembly and disassembly (Fig. 2d), we calculate the average energy of the system as a function of the type-2 monomer content (Fig. 3a, turquoise curve). We then compute the same quantity by sampling configurations where we force monomers of type 2 to bind on their own, without preceding subunits (grey curve). The binding of only tight helical-shaped monomers shows the presence of a high energy barrier, which is completely erased when the whole $0 \to 1 \to 2$ subunit sequence is invoked. The transient presence of the lower-curvature monomer types deforms the membrane enough to ensure the tight helical monomers can bind without having to dramatically bend the membrane from flat to highly indented in one step. This is confirmed by 2D, time-dependent plots of the energy landscape as shown in Fig. S5, where we vary the fraction of monomers of type 1 and 2, keeping the fraction of type-0 monomers constant. At the end of the process, the system ends up in the global energy minimum with only tight helical monomers bound, but to reach this state a threshold number of intermediate type-1 monomers have to bind in order to overcome the energy barrier. As a consequence, the complete sequential assembly renders the whole process faster (Fig. S3).

It should be noted that if the adhesion energy is high enough, tight helical monomers could in principle overcome the binding barrier and deform the membrane spon-

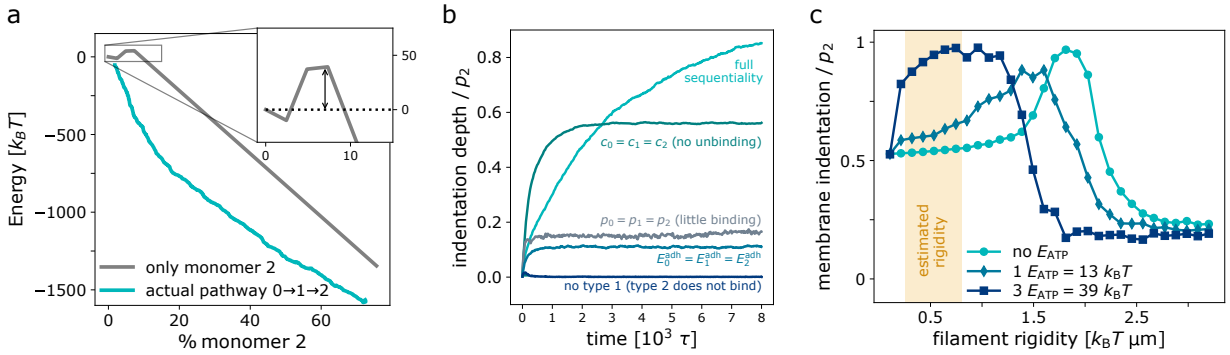

FIG. 3. **Sequentiality and membrane deformation.** (a) The energy of the system as a function of type-2 monomers in the filament, when the full 0-1-2 sequence is present (turquoise), and when monomer 2 is the only one present (grey). The inset shows an energy barrier of 39 k_BT for membrane-bound polymerisation of monomer 2 when no other subunits are involved. (b) Dependence of membrane deformation on monomer unbinding. If the earlier monomer types do not unbind ($c_0 = c_1 = c_2$), the membrane indentation is decreased. In all the other cases ($p_0 = p_1 = p_2$, $E_0^{adh} = E_1^{adh} = E_2^{adh}$), type-2 monomers do not dominate in the final filament. The largest membrane deformation is achieved with full sequential binding and unnbinding. (c) Absence of activity in our model (in turquoise), leads to sequentiality and optimal membrane indentation only for very large filament rigidities. Releasing a sufficiently large energy E_{ATP} to elastically frustrated monomers recovers large indentation at physiologically relevant rigidities, estimated from experiments and models [12, 17] (orange band).

taneously. However, if there is an upper limit to the adhesion energy, as expected in any supramolecular system, then the only way that a filament with a large pitch can deform the membrane into a tube is to ensure that sequentially binding filaments undergo stepwise increases in pitch. We speculate that this upper limit is due either to the chemical details of the membrane interaction, or that Vps4 needs to be able to disassemble the filament in the last stages of neck fission, which would be prohibited by large membrane binding.

Although these data show that the presence of multiple monomer types renders the binding of a highly membrane-deforming filament possible through lowering the energy barrier, this does not explain why earlier monomer types also need to unbind. Fig. 3b shows the depth of membrane indentation for different cases where monomer unbinding is suppressed. In this case, the final composition of the filament is different from the target one (type-2 monomers only) and, as a consequence, the membrane indentation is reduced. We conclude that unbinding of monomers of lower curvatures and pitches optimises the mechanical action of the filament on the membrane.

Role of activity. All the parameters in our model are physiologically realistic (SI table S1), except for the bending rigidity of the filament. To reproduce the unbinding sequence observed in experiment, we find that our filament rigidity needs to be between 3 and 7-fold larger than previously estimated values [12, 17]. However, our passive model does not account for active energy supply, while in experiments dynamic disassembly is only observed upon addition of ATPase Vps4 [5, 18–20]. We set out to understand if a Vps4-like energy consumption in the model could re-create the sequential curves for a physiologically realistic filament rigidity. It is not unreasonable to expect that Vps4 facilitates stress-dependent disassembly. We therefore extended the model so that a monomer with a bending stress above a certain threshold receives one or more external energy portions E_{ATP}, rendering it more likely to unbind. Fig. 3c shows that maximal membrane indentation can be recovered for physically realistic values of the filament rigidities ($< 0.8\, k_BT\,\mu m$) if energy is provided to frustrated monomers. The energy to be supplied was approximately $3E_{ATP} \sim 39\, k_BT$, which is consistent with the energy released by triple-ATP ATPases such as Vps4. Our findings are hence in line with the hypothesis that frustrated subunits in heterogeneous polymers could be more favourably exposed to Vps4, which in turn preferentially extracts them from the polymer [8].

Discussion. In this work we have shown it is possible to produce a membrane-deforming force by staged assembly and disassembly of nanoscale filaments. The system we propose is essentially a dynamic shape-shifting metamaterial: a filament that changes its properties in time to perform a function that each of its parts could not do individually. The overall effect is a membrane-bound elastic structure that with time becomes ever more curved and generates an increasingly deformed membrane. The dynamics of the structure is governed by the properties of the composite monomers and by membrane mechanics. The minimal system for creating a deep indentation of the membrane requires subunits with different binding energies, preferred curvatures, and preferred membrane indentations, which lower the energy barriers for binding and produce optimal indentation.

Here we have considered only three types of monomers, however, including more monomer types can further lower the minimum adhesion energy for the last filament. Nevertheless, adding more monomer exchanges costs additional time and adds a complexity cost. It is to be expected that there is an optimal number of subunits that

maximizes the overall rate for membrane deformation by minimizing the energy barriers and number of steps in tandem.

Within our framework, the unbinding of earlier subunits is caused by filament frustration. This frustration could be realised in different ways: different filament curvatures, which we have used in this work, but it could also enter from different torsion rigidities (SI Fig. S6) or a mixture of curvature difference and bending rigidity difference. In reality, it is likely a mixture of all three. Finally, there is mounting evidence that the membranes mechanical properties regulate ESCRT-III function by affecting the binding dynamics of the subunits [21–23], and possibly that ESCRT-III subunits are also curvature-sensing [24]. Our model quantitatively supports this hypothesis, as subunits are more likely to bind to a membrane that is already deformed according to the filament's preferred morphology.

Acknowledgements. This work has received funding by the European Research Council (ERC) under the European Union's Horizon 2020 research and innovation programme (Grant No. 802960) and from the European Union's Horizon 2020 research and innovation programme under the Marie Skłodowska-Curie grant agreement No. 101034413. A.Š. acknowledges support from the Royal Society (Grant No. UF160266).

[1] M. Vietri, M. Radulovic, and H. Stenmark, The many functions of ESCRTs, Nature Reviews Molecular Cell Biology **21**, 25 (2020).

[2] J. McCullough, A. Frost, and W. I. Sundquist, Structures, Functions, and Dynamics of ESCRT-III/Vps4 Membrane Remodeling and Fission Complexes, Annual Review of Cell and Developmental Biology **34**, 85 (2018).

[3] G. Tarrason Risa, F. Hurtig, S. Bray, A. E. Hafner, L. Harker-Kirschneck, P. Faull, C. Davis, D. Papatziamou, D. R. Mutavchiev, C. Fan, L. Meneguello, A. Arashiro Pulschen, G. Dey, S. Culley, M. Kilkenny, D. P. Souza, L. Pellegrini, R. A. M. de Bruin, R. Henriques, A. P. Snijders, A. Šarić, A.-C. Lindås, N. P. Robinson, and B. Baum, The proteasome controls ESCRT-III–mediated cell division in an archaeon, Science **369**, eaaz2532 (2020).

[4] Y. Olmos and J. G. Carlton, The ESCRT machinery: New roles at new holes, Current Opinion in Cell Biology **38**, 1–11 (2016).

[5] B. E. Mierzwa, N. Chiaruttini, L. Redondo-Morata, J. Moser Von Filseck, J. König, J. Larios, I. Poser, T. Müller-Reichert, S. Scheuring, A. Roux, and D. W. Gerlich, Dynamic subunit turnover in ESCRT-III assemblies is regulated by Vps4 to mediate membrane remodelling during cytokinesis, Nature Cell Biology **19**, 787 (2017).

[6] L. Harker-Kirschneck, B. Baum, and A. Šarić, Changes in ESCRT-III filament geometry drive membrane remodelling and fission in silico, BMC Biology **17**, 1–8 (2019).

[7] H. C. Nguyen, N. Talledge, J. McCullough, A. Sharma, F. R. Moss, J. H. Iwasa, M. D. Vershinin, W. I. Sundquist, and A. Frost, Membrane constriction and thinning by sequential ESCRT-III polymerization, Nature Structural and Molecular Biology **27**, 392 (2020).

[8] A. K. Pfitzner, J. Moser von Filseck, and A. Roux, Principles of membrane remodeling by dynamic ESCRT-III polymers, Trends in Cell Biology **31**, 856 (2021).

[9] A. K. Pfitzner, V. Mercier, X. Jiang, J. Moser von Filseck, B. Baum, A. Šarić, and A. Roux, An ESCRT-III Polymerization Sequence Drives Membrane Deformation and Fission, Cell **182**, 1140 (2020).

[10] X. Jiang, L. Harker-kirschneck, and C. Vanhille, Modelling Membrane Reshaping by Sequential ESCRT-III Polymerization, Unpublished (2021).

[11] W. M. Henne, N. J. Buchkovich, Y. Zhao, and S. D. Emr, The endosomal sorting complex ESCRT-II mediates the assembly and architecture of ESCRT-III helices, Cell **151**, 356 (2012).

[12] Q. T. Shen, A. L. Schuh, Y. Zheng, K. Quinney, L. Wang, M. Hanna, J. C. Mitchell, M. S. Otegui, P. Ahlquist, Q. Cui, and A. Audhya, Structural analysis and modeling reveals new mechanisms governing ESCRT-III spiral filament assembly, Journal of Cell Biology **206**, 763 (2014).

[13] S. T. Huber, S. Mostafavi, S. A. Mortensen, and C. Sachse, Structure and assembly of ESCRT-III helical Vps24 filaments, Science Advances **6**, 1–12 (2020).

[14] J. Moser von Filseck, L. Barberi, N. Talledge, I. E. Johnson, A. Frost, M. Lenz, and A. Roux, Anisotropic ESCRT-III architecture governs helical membrane tube formation, Nature Communications **11**, 1–9 (2020).

[15] M. Alqabandi, N. de Franceschi, S. Maity, N. Miguet, M. Bally, W. H. Roos, W. Weissenhorn, P. Bassereau, and S. Mangenot, The ESCRT-III isoforms CHMP2A and CHMP2B display different effects on membranes upon polymerization, BMC Biology **19**, 1–18 (2021).

[16] R. Dimova, Recent developments in the field of bending rigidity measurements on membranes, Advances in Colloid and Interface Science **208**, 225 (2014).

[17] N. Chiaruttini, L. Redondo-Morata, A. Colom, F. Humbert, M. Lenz, S. Scheuring, and A. Roux, Relaxation of Loaded ESCRT-III Spiral Springs Drives Membrane Deformation, Cell **163**, 866 (2015).

[18] S. Lata, Helical Structures of ESCRT-III are Disassembled by VPS4, Sciencel 10.1126/science.1161070. (2008).

[19] B. A. Davies, I. F. Azmi, J. Payne, A. Shestakova, B. F. Horazdovsky, M. Babst, and D. J. Katzmann, Coordination of substrate binding and ATP hydrolysis in Vps4-mediated ESCRT-III disassembly, Molecular Biology of the Cell **21**, 3396 (2010).

[20] S. Maity, C. Caillat, N. Miguet, G. Sulbaran, G. Effantin, G. Schoehn, W. H. Roos, and W. Weissenhorn, VPS4 triggers constriction and cleavage of ESCRT-III helical filaments, Science Advances **5**, 10.1126/sciadv.aau7198 (2019).

[21] V. Mercier, J. Larios, G. Molinard, A. Goujon, S. Matile, J. Gruenberg, and A. Roux, Endosomal membrane tension regulates ESCRT-III-dependent intra-lumenal vesicle formation, Nature Cell Biology **22**, 947 (2020).

[22] J. Lafaurie-Janvore, P. Maiuri, I. Wang, M. Pinot, J. B.

Manneville, T. Betz, M. Balland, and M. Piel, ESCRT-III assembly and cytokinetic abscission are induced by tension release in the intercellular bridge, Science **340**, 1625 (2013).

[23] A. Booth, C. J. Marklew, B. Ciani, and P. A. Beales, In Vitro Membrane Remodeling by ESCRT is Regulated by Negative Feedback from Membrane Tension, iScience **15**, 173 (2019).

[24] B. Nepal, A. Sepehri, and T. Lazaridis, Mechanisms of negative membrane curvature sensing and generation by ESCRT III subunit Snf7, Protein Science **29**, 1473 (2020).